Published in final edited form as:

Circulation. 2022 September 13; 146(11): 851–867. doi:10.1161/CIRCULATIONAHA.122.060454.

Loss of nuclear envelope integrity and increased oxidant production cause DNA damage in adult hearts deficient in PKP2: a molecular substrate of ARVC

Marta Pérez-Hernández, PhD[1,#], **Chantal J.M. van Opbergen, PhD**[1,#], **Navratan Bagwan, PhD**[2,#], **Christoffer Rasmus Vissing, MD**[3,#], **Grecia M. Marrón-Liñares, PhD**[1], **Mingliang Zhang, PhD**[1], **Estefania Torres Vega, PhD**[2], **Andrea Sorrentino, PhD**[2], **Lylia Drici, PhD**[4], **Karolina Sulek, PhD**[4], **Ruxu Zhai, MS**[5], **Finn B. Hansen, PhD**[2], **Alex Hørby Christensen, MD, PhD**[3,6], **Søren Boesgaard, MD, DMSc**[3], **Finn Gustafsson, MD, DMSc**[3], **Kasper Rossing, MD, DMSc**[3], **Eric M. Small, PhD**[7], **Michael J. Davies, PhD**[2], **Eli Rothenberg, PhD**[8], **Priscila Sato, PhD**[5], **Marina Cerrone, MD**[1], **Thomas Hartvig Lindkær Jensen, MD, PhD**[3], **Klaus Qvortrup, PhD**[2], **Henning Bundgaard, MD, DMSc**[3,*], **Mario Delmar, MD, PhD**[1,*], **Alicia Lundby, PhD**[2,*]

[1:]The Leon H Charney Division of Cardiology, NYU-Grossman School of Medicine, New York, United States

[2:]Department of Biomedical Sciences, Faculty of Health and Medical Sciences, University of Copenhagen, Copenhagen, Denmark

[3:]Department of Cardiology, The Heart Centre, Rigshospitalet, Copenhagen, Denmark and Department of Clinical Medicine, University of Copenhagen, Denmark

[4:]The Novo Nordisk Foundation Center for Protein Research, Faculty of Health and Medical Sciences, University of Copenhagen, Copenhagen, Denmark

[5:]College of Medicine, Drexel University, Philadelphia, PA 19102, United States

[6:]Department of Cardiology, Copenhagen University Hospital - Herlev-Gentofte Hospital, Copenhagen, Denmark

[7:]University of Rochester, Aab Cardiovascular Research Institute, Department of Medicine, University of Rochester School of Medicine and Dentistry, Rochester, NY 14642, United States

[8:]Division of Pharmacology, NYU School of Medicine, New York, United States

Abstract

Background.—Arrhythmogenic right ventricular cardiomyopathy (ARVC) is characterized by high propensity to life-threatening arrhythmias and progressive loss of heart muscle. More than 40% of reported genetic variants linked to ARVC reside in a gene called *PKP2*, which encodes the plakophilin-2 (PKP2) protein.

Co-corresponding authors: mario.delmar@nyulangone.org or alicia.lundby@sund.ku.dk.
[#:]Equally contributed first authorship
[*:]Equally contributed last authorship

DISCLOSURES:
None.

Methods.—We describe a comprehensive characterization of the ARVC molecular landscape as determined by high-resolution mass spectrometry, RNA sequencing and transmission electron microscopy of right ventricular biopsy samples obtained from ARVC patients with PKP2 mutations and left ventricular ejection fraction (LVEF) above 45%. Samples from healthy relatives served as controls. The observations led to experimental work using multiple imaging and biochemical techniques in mice with a cardiac-specific deletion of *Pkp2* studied at a time of preserved LVEF, and in human induced pluripotent stem cell-derived PKP2-deficient myocytes (hiPSC-CM-PKP2KOs).

Results.—Samples from ARVC patients present a loss of nuclear envelope integrity, molecular signatures indicative of increased DNA damage and a deficit in transcripts coding for proteins in the electron transport chain. Mice with a cardiac-specific deletion of *Pkp2* also present a loss of nuclear envelope integrity, which leads to DNA damage and subsequent excess oxidant production ($O_2^{\bullet-}$ and H_2O_2), the latter further increased under mechanical stress (isoproterenol or exercise). Increased oxidant production and DNA damage is recapitulated in hiPSC-CM-PKP2KOs. Furthermore, PKP2-deficient cells release H_2O_2 into the extracellular environment, causing DNA damage and increased oxidant production in neighboring myocytes in a paracrine manner. Treatment with Honokiol increases mitochondrial NAD-dependent protein deacetylase sirtuin-3 activity, reduces oxidant levels and DNA damage *in vitro* and *in vivo*, reduces collagen abundance in the right ventricular free wall and has a protective effect on right ventricular function.

Conclusions.—Loss of nuclear envelope integrity and subsequent DNA damage is a key substrate in the molecular pathology of ARVC. We further show transcriptional downregulation of proteins of the electron transcript chain as an early event in the molecular pathophysiology of the disease (prior to loss of LVEF<45%), which associates with increased oxidant production ($O_2^{\bullet-}$ and H_2O_2). We propose therapies that limit oxidant formation as a possible intervention to restrict DNA damage in ARVC.

Keywords

arrhythmogenic right ventricular cardiomyopathy; plakophilin 2; nuclear envelope; DNA damage; oxidative stress; SIRT3

INTRODUCTION

Arrhythmogenic right ventricular cardiomyopathy (ARVC) is an inherited cardiac disorder characterized by high propensity to life-threatening arrhythmias and progressive loss of heart muscle.[1,2] ARVC is the second most common cause of unexpected sudden death by cardiac arrest in the young. The cardiomyopathy can be progressive and patients often require pharmacotherapy, ablation therapy, intracardiac defibrillators and in terminal cases, a heart transplant to prevent death.

More than 40% of reported genetic variants linked to ARVC reside in a gene called *PKP2*, encoding the plakophilin-2 (PKP2) protein.[3,4] PKP2 is classically defined as a protein of the desmosome, an intercellular adhesion structure residing at the intercalated disc. Recent work shows that PKP2 also regulates the function of the cardiomyocyte itself, and that

loss of these cell-intrinsic functions leads to a disease phenotype.[5-7] Yet, knowledge on the molecular consequences of PKP2 deficiency has, for the most part, been limited to experimental models.

Here, we describe a comprehensive characterization of the ARVC molecular landscape as determined by high-resolution mass spectrometry, RNA sequencing and transmission electron microscopy (TEM) of right ventricular (RV) biopsy samples obtained from ARVC patients with *PKP2* mutations and their healthy relatives. The results prompted us to postulate that PKP2 deficiency leads to activation of the DNA damage response (DDR) via disruption of nuclear envelope structural integrity and, separately, enhanced formation of reactive oxidants commonly termed “reactive oxygen species” (ROS). Experimental results obtained in a murine model of PKP2 deficiency and in human induced pluripotent stem cell-derived cardiomyocytes (hiPSC-CMs) with reduced abundance of PKP2 supported this hypothesis. We propose a novel mechanism of PKP2-dependent ARVC centered on DNA damage resulting from structural disruption of the nuclear envelope, and we identify and evaluate a potential target for treatment based on activating mitochondrial deacetylase sirtuin-3 (SIRT3).

MATERIAL AND METHODS

Biopsies were obtained from the right ventricle (RV) of five patients with ARVC diagnosis (carriers of pathogenic PKP2 variants). Control samples originated from three healthy, non-variant carrier relatives. The study was approved by the Institutional Review Board, the Ethics Committee of the Capital Region of Denmark (H-17034423); all subjects gave written informed consent to participate. Animal experiments were performed in 3-4 month old mice expressing a cardiac-specific deletion of PKP2 (PKP2cKO). Procedures conformed with the Guide for Care and Use of Laboratory Animals of the National Institutes of Health and were approved by the NYU-IACUC committee.

All procedures are detailed in the Supplement. Mass spectrometry proteomic data were deposited in the ProteomeXchange Consortium via PRIDE repository (dataset identifier PXD025523, accessible through https://www.ebi.ac.uk/pride/archive), project name “arrythmogenic right ventricular cardiomyopathy (PKP2-cKO in mice and Human biopsies)”. Danish law precludes public distibution of FASTQ files from human RNA-seq experiments (see also Supplemental Methods). Additional information can be made available from the corresponding authors upon reasonable request.

Statistical analysis

Data that passed a test for normality were analyzed by Student’s t-test, ANOVA, or linear mixed effects analysis (for nested data). Data not normally distributed were tested by Mann Whitney, or by a generalized linear mixed model analysis (nested data). Specifics on analysis of each dataset are noted in the figure legends. Data are reported as Mean plus/minus Standard Deviation of the Mean. Statistical significance was set for $p<0.05$. n values (number of events) and N values (number of individuals) are specified for each dataset in figure legends.

RESULTS

Clinical characteristics of biopsy donors

Septal endomyocardial biopsies were obtained transvenously from the RV of five patients, ages 18 to 55 with diagnosis of ARVC as per 2010 taskforce criteria.[8] Patients were carriers of a pathogenic *PKP2* variant and had a left ventricular ejection fraction (LVEF) of more than 45% at the time samples were collected. Equivalent samples from three healthy, non-variant carrier relatives to patients with ARVC were used as control. Major clinical characteristics of ARVC patients are presented in Table 1. The study was approved by the Ethics Committee for the Capital Region Copenhagen (H-17034423). Additional clinical information is provided in Table S1 and in Supplementary Material. Pedigrees and representative electro- and echocardiograms for each ARVC patient are shown in Supplementary Figs.S1-S3. Cardiac biopsies were prepared for subsequent analyses immediately upon collection, with samples handled individually for: i) TEM, ii) light microscopy (LM), iii) RNA sequencing, and iv) proteomics.

PKP2 deficiency negatively impacts nuclear envelope integrity

Transmission electron microscopy (TEM) images acquired from heart samples collected from ARVC patients revealed structural differences in cardiomyocyte nuclei. Figure 1A shows exemplary TEM images from a healthy control (top) and from an ARVC patient (bottom). In the control, the nuclear envelope presented a continuous, smooth appearance. In cardiomyocytes from ARVC patients the nuclear envelope appeared convoluted, with extensive invaginations (infoldings), yielding a normalized perimeter that was statistically different from that of controls (Fig.1B). In heart samples from ARVC patients we also noted areas of the nuclear envelope crowded by adjacent mitochondria, and sites where the nuclear membrane lost continuity, allowing underlying chromatin to be observed outside of the nuclear perimeter (Supplementary Fig.S4), a morphology not observed in controls. Neural network-based evaluation of LM images of Haematoxylin-stained thin sections identified the origin of the samples as those collected from ARVC patients (versus controls) with 85% accuracy. Morphometric analysis showed that nuclear size was larger in cardiomyocytes from ARVC patients than in controls (Fig.1C-D). Similar results were obtained in a murine model of cardiomyocyte-specific, tamoxifen (TAM)-activated *Pkp2* gene deletion (PKP2cKO; see “Methods” and[6]). Neural network-based evaluation of LM images of Haematoxylin-stained thin sections discerned images collected from PKP2cKO mice versus controls with 97% accuracy, and morphometric analysis showed that nuclei of PKP2cKO cardiomyocytes were larger than those from controls (Supplementary Fig.S5A).

The link between changes in nuclear morphology and PKP2 expression was further evaluated in PKP2cKO hearts. Confocal microscopy analysis showed that the nuclear envelope of PKP2cKO myocytes presented multiple invaginations (Fig.1E), reminiscent of the infoldings of nuclear envelope described by Heffler et al in the context of reduced desmin expression.[9] Consistent with an increase in invaginations, the signal intensity of lamin-B1-stained myocyte nuclei was increased in PKP2cKO specimens when compared to controls (Fig.1F). Average nuclear size in isolated PKP2cKO myocytes was also larger than in controls (Supplementary Fig.S5B).

To test whether changes in nuclear morphology associated with changes in the efficiency of the nuclear membrane to act as a barrier we implemented the method described by Ljubojevic *et al.*[10] Calcium (Ca^{2+}) transients were recorded from the central and the nucleolemmal parts of the nucleus, and the difference in time to peak of the transients was taken as indicative of the diffusional capacity of Ca^{2+}through the nuclear compartment. As displayed in Fig.1G, the difference in time to peak was less in PKP2cKO myocytes when compared to controls, indicating less impeded Ca^{2+}flux from the nuclear envelope to the center of the nucleus consequent to loss of PKP2. Consistent with this observation, there was no significant gradient in diastolic Ca^{2+} between the center and nucleolemmal region in PKP2cKO myocytes (Supplementary Fig.S5C). To put these results into context, the data led us to speculate that in parallel to, and perhaps preceding, previously identified molecular pathways leading to transcriptional dysregulation in ARVC[6,7], ARVC associates with a loss of nuclear envelope integrity and subsequent activation of the DNA damage response.

PKP2 deficiency associates with increased levels of γH2AX, a marker of DNA damage

Disruption of nuclear envelope integrity results in DNA damage.[11,12] We evaluated the relation between PKP2 expression and DNA damage in isolated PKP2cKO myocytes by quantification of γH2AX, an early component of the DNA damage response.[13] As displayed in Fig.2A-C, the immunofluorescent γH2AX signal intensity, and the abundance of immunodetectable γH2AX clusters, were increased in PKP2cKO myocytes compared to controls. Finally, to confirm that increased DNA damage can be ascribed directly to PKP2 deficiency in myocytes, we quantified γH2AX in hiPSC-CMs lacking PKP2 (Fig.2D-F). Positive controls for DNA damage in cardiomyocytes by γH2AX are shown in Supplementary Figure S6A-B for ventricular myocytes, and Supplementary Figure S6C-D for hiPSC-CMs. The overall results, based on two independent experimental systems, show that loss of PKP2 expression results in increased DNA damage in cardiomyocytes.

Molecular signatures of DNA damage in ARVC patient heart samples

Our results led us to search for molecular evidence of DNA damage in ARVC-affected human hearts. To quantitatively evaluate the molecular profile of human cardiac tissue we applied unbiased omics approaches (deep quantitative proteomics and transcriptomics). For proteomics, we extracted proteins through a combination of tissue homogenization, solubilization and sonication followed by enzymatic digestion.[14,15] Peptides were labelled with chromatographically indistinguishable isobaric TMT tags[16,17], separated into 46 fractions by high-pH reversed-phase fractionation and measured by high-resolution mass spectrometry. The resulting proteome dataset comprised 67,033 sequence-unique peptides accounting for 6,181 proteins with an average protein sequence coverage of 24% (Fig.3A, Supplementary Fig.S7A). Technical reproducibility was excellent, with average Pearson correlation coefficients of 0.98 (range 0.95-0.99) for protein intensities across biological replicates (Supplementary Fig.S7B). This is an unprecedented depth of analysis of human heart protein abundances in the setting of ARVC. To identify differential expression, for each protein measured we plotted its p-value as a function of protein intensity difference between logarithmized means of ARVC patients and controls (Fig.3B; data from Supplementary Table-S2). This allowed identification of proteins more abundant in hearts of ARVC patients compared to controls (e.g., desmin, Des) as well as those with

reduced abundance (e.g., PKP2 and other desmosomal proteins). The data were analyzed using gene set enrichment analysis[18] to identify hallmark pathways[19], which were either over- or underrepresented in ARVC heart samples (Fig.3C). We found overrepresentation of pathways involved in DNA damage (UV response, P53 pathway, KRAS signaling and G2M checkpoint) and in 'Apoptosis' and 'Reactive oxygen species (ROS)' pathways, including proteins that remove or prevent excess oxidant formation. Separate analysis of transcriptomics data highlighted many of the same pathways, namely, upregulation of apoptosis and DNA damage response, and downregulation of oxidative phosphorylation (Fig.3D, data in Supplementary Table-S3). Guided by the molecular fingerprint of a DNA damage response, we observed in our dataset an enrichment for proteins known to be recruited to DNA repair hotspots at sites of DNA double-stranded breaks[20] (Fig.3E). Altogether, these omics analyses of human heart samples support the notion of increased DNA damage in ARVC hearts with PKP2 deficiency.

DNA damage occurs independently of a significant increase in oxidant levels

Heffler *et al* showed that the structure of the nuclear envelope is maintained by the balance of forces exerted by intermediate filaments (desmin in the case of myocytes) and the microtubules, and that disruption of this balance is deleterious to the integrity of the nuclear envelope and the underlying chromatin, thereby triggering a DNA damage response that is independent of oxidant formation.[9] Given the relation between desmin and the desmosome[21], we investigated whether desmin anchoring at the cell end was disrupted in PKP2cKO cardiomyocytes, and whether this would also manifest in a disruption of desmin anchoring to its nuclear envelope scaffolding. Single molecule localization microscopy (SMLM) showed that the distance between desmin and the cell end (marked by N-Cadherin), and between desmin and the nuclear envelope (marked by lamin-B1) were significantly increased in PKP2cKO myocytes (Fig.4A-B; complete data distribution profile presented in Supplementary Fig.S8A). This increase occurred despite the fact that desmin clusters, measured throughout the cell, were larger and more elongated in PKP2cKO cardiomyocytes than in controls, and that desmin protein abundance was increased in PKP2cKO hearts (Supplementary Fig.S8B-C), as was also the case in hearts of ARVC patients (Fig.3B). Finally, consistent with data showing that altered nuclear morphology is a consequence of reduced desmin attachment[22], we observed that nuclei of PKP2cKO myocytes were more circular than those of controls (Fig.4C).

Nuclear morphology is maintained by the balance between the pull force applied by intermediate filaments on the nuclear envelope, and the "push" force applied by dynamic microtubules as they grow and interact with their nuclear envelope attachment.[9] Accordingly, we examined whether limiting microtubule polymerization by colchicine would rescue nuclear envelope morphology(as in[9]). Mini-osmotic pumps were loaded with colchicine (0.4 mg/kg/d) and implanted on day 7 after TAM injection (Fig.4D). At day 21 post-TAM, mice were euthanized, cardiomyocytes dissociated and myocyte nuclei stained for laminB1 and DAPI, to evaluate nuclear dimensions and circularity. Colchicine administration led to decreased laminB1 intensity and reduced nuclear circularity (Fig.4E). These results are consistent with those of Heffler *et al.* when characterizing the effect of

desmin knockout, and with the notion that in PKP2cKO hearts, desmin distances itself from its anchoring points (Fig. 4A-B).

We speculated that a positive inotropic agent could, by increasing mechanical stress on the cytoarchitecture, accentuate the PKP2-dependent DNA damage in an oxidant-independent manner. Thus, we subjected PKP2cKO mice to three boluses of isoproterenol (ISO), at 30 minute intervals. Acute ISO exposure did not cause increased oxidant production in PKP2cKO myocytes (Supplementary Fig.S9). Yet, ISO induced a significant increase in γH2AX intensity (Fig.4F, Supplementary Fig.S10). The results suggest that in the beating heart, DNA damage in PKP2-deficient myocytes can be caused by an oxidant-independent mechanism.

To examine increased adrenergic tone under more physiological conditions, we assessed DNA damage in control and PKP2cKO mice subjected to exercise. Mice were trained for six weeks to run on a treadmill, following a protocol previously validated in our laboratory.[22] The intensity of γH2AX signals recorded from myocytes of exercised animals was compared to that recorded from myocytes of sedentary animals. As shown in Figure 4G, exercise associated with increased DNA damage response in PKP2cKO animals, but not in controls. Of note, increased adrenergic tone and enhanced oxidant production likely occur as a result of the exercise protocol. Additional studies described below focused on the relation between oxidant production and DNA damage in PKP2 deficient myocytes.

Dysregulation of mitochondrial structure/function and increased levels of oxidant production

Independent of (or in parallel to) disrupted nuclear membrane integrity, DNA damage can result from mitochondrial dysfunction and consequent increased oxidants.[23] Data in Fig.3 and Supplemental Fig.S11 suggest that mitochondrial dysfunction is part of the cellular/molecular phenotype of ARVC. This was supported by ultrastructural observations on samples from human ARVC hearts. As shown in Fig.5A and Supplementary Fig.S11A, we found abundant mitochondrial clustering in myocytes, forming large bundles that in some cases occupied large spaces at the expense of other structures. Proteomics analysis of human heart samples revealed a general downregulation of mitochondrial proteins (Supplementary Fig.S11B), including those involved in the electron transport chain and the ATP synthase (Supplementary Fig.S11C). The large number of mitochondria and yet reduced abundance of mitochondrial proteins is consistent with previous studies in other cardiomyopathies.[24] To evaluate mitochondrial function in PKP2 deficient myocytes, we measured oxygen consumption rates (OCR) in cardiomyocytes from PKP2cKO mice and controls (Fig.5B; Supplementary Fig.S11D). Despite downregulation of proteins in the electron transport chain, basal respiration was not significantly affected. Yet, maximal respiration was decreased in PKP2cKO myocytes, suggesting diminished capacity to accommodate high oxidative energy demand (e.g., in exercise). ATP-linked respiration and proton leak were decreased and increased respectively, overall supporting the notion of functionally impaired mitochondria. These changes are likely exacerbated during high bioenergetic demand and contribute to cardiomyocyte dysfunction. Based on our results, we investigated whether PKP2 deficiency correlates with enhanced oxidant production in our experimental models.

To this end, we labelled myocytes with either MitoSOX (adult ventricular myocytes) or CellROX (hiPSC-CMs; examples in Supplementary Fig.S12) and fluorescence intensity was evaluated as an indicator of oxidant generation. Figure 5C-D shows the results. We observed significantly higher levels of oxidant generation in PKP2cKO myocytes and PKP2KO hiPSC-CMs compared to controls. Collectively, deficiency in PKP2 coupled, directly or indirectly, to increased oxidant production in cardiomyocytes.

Intercellular propagation of DNA damage response by hydrogen peroxide (H_2O_2)

Previous studies show that loss of PKP2 in a cell can impact others distal to it, even if the distal cells do express PKP2[25], suggesting that loss of PKP2 can lead to paracrine regulation of distant neighbors. To test whether oxidant production and DNA damage can propagate from PKP2-KO to PKP2-expressing cells, we recovered culture media from PKP2KO hiPSC-CMs (conditioned media) and transferred it to control hiPSC-CMs (Fig.5E). Incubation in conditioned media led to increased oxidant levels and DNA damage in recipient control cells (Fig.5F-G; Supplementary Fig.S13). In contrast, media from control cells did not elicit either oxidant or DNA damage signaling in recipient controls (Fig.5F-G). Based on the oxidant signaling proteins upregulated in human hearts (highlighted in Fig.3C) we inferred that the likely mediator of these effects was H_2O_2. Consistent with the latter, levels of H_2O_2 in conditioned media originating from PKP2-KO cells were significantly higher than in media from control cells (Fig.5H). Furthermore, pre-treating conditioned media with catalase, an enzyme that degrades H_2O_2 with high selectivity, mitigated the enhanced oxidant production in recipient cells (Fig.5I). Overall, these data suggest that H_2O_2 is released into the extracellular environment by PKP2-deficient cells and may, in turn, act as a messenger to propagate DNA damage to cells with preserved PKP2 expression.

Activation of SIRT3 reduces oxidant and DNA damage and rescues phenotype

Given the relation between oxidant production and DNA damage response, we sought to identify potential targets for treatment. Of particular interest was Sirt3, a mitochondrial deacetylase which a) functions as an oxidant removal agent in cardiac myocytes[26,27], b) was found to be reduced in the proteomic analysis of ARVC human hearts and of PKP2cKO mice (Fig.3B, Supplementary Fig.S14A), and c) can be pharmacologically activated by the conjugated biphenolic compound Honokiol.[28,29] The reduction in SIRT3 expression was also observed at the transcriptional level both in PKP2cKO mice and in hiPSC-CM lacking PKP2 (Supplementary Fig.S14B).

Exposing PKP2-deficient hiPSC-CMs for 24 hours to 10 μmol/L Honokiol significantly decreased oxidant levels and γH2AX signals (Fig.6A-C). Separately, we examined the effect of Honokiol (2mg/kg/day) in PKP2cKO animals treated for 14 days starting on day 7 post-TAM (Fig.6D). Honokiol reduced oxidant production and γH2AX signal intensity in cardiomyocytes of PKP2cKO animals when compared to cardiomyocytes from vehicle-injected PKP2cKO mice (Fig.6E-F). In vitro analysis showed reduced Sirt3 enzymatic activity in PKP2cKO hearts compared to control, and rescue of Sirt3 activity in PKP2cKO hearts treated with Honokiol (Fig.6G). Echocardiographic evaluation showed amelioration of the increase in RV area characteristic of PKP2-deficient hearts at this stage[6] and

concurrent decrease in RV collagen abundance in the treated hearts (Fig.6H-I). LVEF and fractional shortening were not significantly affected (Supplementary Fig.S15), as expected for this stage of disease progression in PKP2cKO mice, where LV contractile deficit and fibrosis are minor or not significant.[6]

DISCUSSION

We characterized the subcellular structure and molecular profile of RV septal tissue collected from patients that met 2010 task force criteria for diagnosis of ARVC and carried a PKP2 variant classified as pathogenic, but whose LVEF remained above 45%. In addition, collected samples from healthy relatives. The latter, together with the depth of our proteomics analysis, allowed us to characterize the differential proteome and transcriptome of cardiac tissue from humans with ARVC at an unprecedented level. Our results, supported by various experimental approaches both in adult murine hearts and in human iPSC-CMs deficient in PKP2, lead us to propose that activation of the DNA damage response is critical to the molecular phenotype of PKP2-dependent ARVC, that this process is initiated by nuclear envelope disruption leading to chromatin disorganization and DNA damage, deficit in transcripts coding for proteins involved in the electron transport chain, and consequent increased production of mitochondrially-derived oxidants. The model is diagrammatically represented in Figure 7.

We found reduced abundance of proteins involved in the electron transport chain in tissue from ARVC patients (Supplementary Fig.S11C), suggesting impaired function. and enhanced formation of superoxide radical anions ($O_2^{\bullet-}$) from partial (incomplete) reduction of molecular oxygen (O_2) upstream of Complex IV. Rapid spontaneous or enzyme catalyzed (by superoxide dismutases) $O_2^{\bullet-}$ yields the observed increase in H_2O_2. Accordingly (Fig.3C), we observed increased abundance of proteins involved in the removal of $O_2^{\bullet-}$ (SOD1), H_2O_2 (CAT), peroxiredoxins (PRDX2, PRDX4) and phospholipid hydroperoxides [GPX4], in maintenance of the thiol pool in a reduced form (TXN, TXNRD1, GLRX2, GCLM) and in reduction of oxidized peroxiredoxins (SRXN1). Transcript increases were also detected for proteins involved in binding and control of redox-active metal ions (FTL, ATOX1). Some of these proteins are mitochondrial isoforms [GLRX2, SRXN1] consistent with the observed mitochondrial dysfunction, but others are cytosolic (SOD1, PRDX2, TXN), peroxisomal (CAT), or associated with membranes (GPX4) consistent with widespread (delocalized) intracellular oxidative stress and our detection of H_2O_2 in the cell media. These increases likely result from transcriptional signaling, as mRNA levels were also elevated. We have therefore captured a snapshot of the human heart affected with ARVC at a point in which oxidant production is elevated, but with active transcriptionally-initiated responses to limit oxidant damage. Our results help untangle the timing of events that lead to increased apoptosis as previously reported in human hearts and myocytes.[3,30-33] Rather than excess oxidant formation resulting from deficit of proteins involved in oxidant removal, we suggest that increased oxidant production ($O_2^{\bullet-}$ and H_2O_2) initially occurs despite elevated levels of protective proteins, and that deficit in transcripts coding for proteins involved in the electron transport chain is an early event affecting mitochondrial function. We further speculate that balance between these two factors (elevated protective

proteins compensating for reduced ETC components) can be broken by further strain to the heart (e.g., high-intensity sports; age) leading to structural and functional derangements.

The question remains as to the cause of the initial transcriptional deficit. We demonstrate that PKP2 deficit in an adult heart is sufficient condition for disrupting nuclear envelope morphology (Fig.1A,E, Fig.4C) and its function as a barrier (Fig.1G). We suggest that these changes are linked to distancing of desmin from its anchoring points, not only at the intercalated disc[34] but critically, at the nuclear envelope, thus impairing the function of desmin as a structural pilar of nuclear architecture. Indeed, it is known that desmin filaments maintain, together with microtubules, a pull-and-push equilibrium over the nuclear envelope that preserves its shape, its barrier function, and the integrity of the underlying chromatin (the lamin-associated domain;[9]). Along those lines, we demonstrate that preventing microtubule polymerization rescues nuclear envelope morphology (Fig.4A-E), consistent with results obtained in a model of desmin knockout.[9] Overall, we propose that desmin acts as a molecule that translates the mechanical stress of the intercalated disc into a transcriptional response, and that it is the PKP2-dependent altered abundance and distribution of desmin which breaks the desmin/microtubule pull/push balance, disrupting the structural architecture of the nuclear envelope and the transcriptional program of the underlying DNA.

The data in Figure 4F show that an adrenergic surge (ISO boluses) is sufficient to initiate DNA damage. We propose the hypothesis that this effect results from the mechanical stress imposed on the cytoskeleton (and consequently, on the nuclear envelope) by the increased strength of contraction, though we cannot completely discard phosphorylation-dependent, inotropy independent effects. Indeed, no experiments were performed to look at mechanical stress transduction as the specific cause of increased DNA damage in this series of experiments. Be it through the increased inotropy or by some other mechanism, what is clear is that DNA damage in a PKP2-deficient myocyte can be independent of elevated oxidant formation. Together with the observation of increased DNA damage in mice subjected to treadmill running (Fig.4G) our data link DNA damage to two known environmental factors (adrenergic surge; endurance exercise) that can impact negatively on the progression of ARVC.

Based on the arguments above, we propose that in the fully-formed, beating heart, the molecular pathology of ARVC is initiated by the mechanical stress imposed on the nuclear envelope by its disrupted mechanical coupling. The latter does not discard the importance of oxidant production in the process. Indeed, increased oxidant generation consequent to desmosomal deficiency is also observed in hiPSC-CMs (Fig.5D) and in embryonic-derived cardiomyocytes[37] and yet these cells are not subject to the tensile forces of an adult myocyte. In that context, it is important to note our previous observation that PKP2 deficiency leads to increased intracellular Ca^{2+}in all compartments, including the mitochondria[7], an event also present in hearts/cells with desmoglein-2 deficiency.[35] We thus propose two mechanisms, one only apparent in the contractile adult heart and related to mechanical disruption of the nuclear envelope and another that is also observed in cultured cells, involving excess entry of Ca^{2+}into the cell and oxidant over-production.

TEM images of ARVC human samples showed large number of mitochondria within the cells, some forming “mitochondrial cysts” on the edges. Mitochondria were also apparent in the intercellular space. The latter is reminiscent of previous studies showing that myocytes shed out mitochondria as a mechanism for renewing the mitochondrial pool.[36] It is tempting to speculate that excessive mitochondrial shedding constitutes a message for activation of the inflammatory and immune responses (as suggested by Nicolas-Avila et al[36]), which have been described in the setting of ARVC.[37] Non-myocytes were clearly apparent in our LM (Fig.1C) and TEM images, and quantitative proteomics of human heart samples pointed to increased abundance of proteins involved in the inflammatory response (Fig.3C). Our data thus support the hypothesis that inflammatory and immune responses are part of the molecular pathophysiology of ARVC at this stage, which presents itself as a potential therapeutic target, to be explored in future studies.

Our studies show that H_2O_2 acts as an intercellular messenger enhancing oxidant production in distal cells (Fig.5E-I). Of note, it is unclear whether paracrine effects of H_2O_2 are important *in vivo* as part of the PKP2 ARVC phenotype; in fact, it is quite possible that intracellular production of H_2O_2 plays the most important role *in vivo*. Whether the paracrine mechanism impacts on the response of non-myocytes to the environment, remains unclear. Our studies also show that reducing H_2O_2 with catalase (Fig.5I) or preventing/reducing oxidant levels with Honokiol (via Sirt3 activation) may be a valid target for therapy. Regarding the latter, Honokiol treatment reduced the extent of DNA damage in cells in culture (Fig.6C) and in adult hearts following a 14-day treatment (Fig.6F). It also decreased fibrosis and mitigated the increase in RV area detected by echocardiography. Honokiol is a natural product, readily available, and previous studies have shown that among its effects is to act as an activator of the mitochondrial deacetylase Sirt3[28,29], a protein that in human ARVC hearts and murine PKP2cKO hearts was found downregulated (Fig.3C, Supplementary Fig.S14). We report that Honokiol treatment rescued Sirt3 activity in PKP2cKO hearts. Thus, this natural and readily available product may offer a protective advantage from ROS damage to the heart. However, in-depth studies would be necessary to validate its safety, efficacy and specificity for use by patients with ARVC.

Because of obvious limitations, we were unable to directly demonstrate DDR in cells of ARVC patients. Yet, the molecular landscape detected by our studies, and data obtained from experimental models, strongly suggest that the conditions are present for increased DDR. Given the relation between DDR and cell senescence, one can conceptualize ARVC as a process where cells age prematurely. In fact, we observed an association between PKP2 deficiency and nuclear envelope integrity. The nuclear envelope is the site of residence of at least two proteins which, when mutated, have been linked to a cardiomyopathy: laminA/C and TMEM43. Interestingly, among those cases, there are reported similarities with the ARVC phenotype. Deficiency in the abundance or primary sequence of both TMEM43 and laminA/C have been linked to increased DDR.[38,39] We speculate that, fundamental differences notwithstanding, DNA damage resulting from structural disruption of the nuclear envelope may help explain similarities between the ARVC phenotype caused by PKP2 mutations, and the phenotype detected in some cases resulting from mutations in laminA/C[40] or TMEM43[41]. Further studies must examine whether mutations in other non-

desmosomal proteins involved in arrhythmogenic cardiomyopathy, such as phospholamban, share this common disease pathway.

DNA damage can be significantly modulated by epigenetic factors (exercise, adrenergic stimulation). Studies show that oxidant production can be modulated by moderate exercise[42] and by dietary habits.[43] The extent to which modulation of oxidant-dependent pathways can be benefitial in healthy individuals and detrimental to others is unknown. What seems clear is that ARVC emerges as a disease that, although inheritable, may be greatly sensitive to life style factors that affect the DNA damage response. Identifying the environmental framework that separates health from disease may be critical for proper management of gene-positive individuals at risk.

A large fraction of our work was conducted in two experimental models of PKP2 deficiency (PKP2cKO mice and PKP2-KO hiPSC-CMs). No experimental model of PKP2 deficiency recapitulates human ARVC in all its features, from the fact that only one allele presents a mutation, to the right-side preference of the cardiomyopathy, the heightened occurrence of sudden cardiac death in the concealed phase, and the epi-to-endo fibroadiposis. Our intention is not “to recapitulate ARVC,” but to better understand the cardiac endophenotype of a gene that, when mutated, produces the disease. For that purpose, we knock out the gene in adult hearts and observe the phenotype that results in the absence of such gene. Our results show similarities between the phenotype after KO, and the one observed in patients with ARVC. We cannot be certain that those similarities point to mechanisms common in PKP2cKO mice and in PKP2-deficient humans, but seems likely. Any extrapolation needs to be done with caution.

In conclusion, we described the molecular and structural landscape of human hearts with ARVC caused by specific (likely loss-of-function) variants in *PKP2*. Our results provide an in-depth picture of the phenotype and provide clues as to the nature of events that lead to clinically overt disease. As summarized in Figure 7, we propose that mechanical forces disrupt the nuclear envelope, causing DNA damage and reduced expression of electron transport chain genes, leading to mitochondrial dysfunction and excess oxidant production (likely $O_2^{\bullet -}$ and hence H_2O_2) even in the background of compensatory overexpression of molecules that remove H_2O_2. We confirm that in cells in culture, loss of PKP2 expression can lead to increased oxidant formation, likely consequent to increased Ca^{2+} levels. Finally, we show that H_2O_2 mediate propagation of DNA damage, and limiting oxidant production may be a plausible therapeutic goal. Further studies will be necessary to elucidate whether treatments that decrease oxidant formation can decelerate the progression of ARVC.

Supplementary Material

Refer to Web version on PubMed Central for supplementary material.

SOURCES OF FUNDING:

This work was supported by a Transatlantic Network of Excellence from the Leducq Foundation to AL and MD, grant R35HL160840 to MD, RO1HL136179 to MD and ES, and grant RO1HL145911 to MD, as well as Postdoctoral Fellowships from the Heart Rhythm Society to CvO and from American Heart Association to CvO and GM-L. The work was also supported by The Danish Council for Independent Research (DFF–0134-00054B)

to AL as well as by The Novo Nordisk Foundation (NNF18OC0052844 and NNF20OC0059767) to AL and (NNF20SA0064214) to MJD. PYS was supported by NIH R56HL149887 and R01HL163666. Support was received from The Innovation Fund Denmark, NordForsk, The AP Møller Foundation, The Research Foundations at Rigshospitalet and at The Capital Region of Denmark to HB. The mass spectrometry measurements were performed at The Novo Nordisk Foundation Center for Protein Research, which is funded in part by a generous donation from the Novo Nordisk Foundation (NNF14CC0001).

Nonstandard Abbreviations and Acronyms

ARVC	arrhythmogenic right ventricular cardiomyopathy
DDR	DNA damage response
hiPSC-CM	cardiomyocytes derived from human induced pluripotent stem cell
ISO	isoproterenol
LVEF	left ventricular ejection fraction
OCR	oxygen consumption rates
PKP2	plakophilin-2
ROS	reactive oxygen species
RV	right ventricle
SIRT3	sirtuin 3
SMLM	single molecule localization microscopy
STORM	stochastic optical reconstruction microscopy
TAM	tamoxifen
TEM	transmission electron microscopy

REFERENCES:

1. Delmar M, McKenna WJ. The cardiac desmosome and arrhythmogenic cardiomyopathies: from gene to disease. Circ Res 2010;107, 700–714. [PubMed: 20847325]
2. Corrado D, Link MS, Calkins H. Arrhythmogenic Right Ventricular Cardiomyopathy. N Engl J Med 2017;376, 61–72. [PubMed: 28052233]
3. Austin KM, Trembley MA, Chandler SF, Sanders SP, Saffitz JE, Abrams DJ, Pu WT. Molecular mechanisms of arrhythmogenic cardiomyopathy. Nat Rev Cardiol 2019;16, 519–537. [PubMed: 31028357]
4. Groeneweg JA, Bhonsale, James CA, te Riele AS, Dooijes, Tichnell, Murray, Wiesfeld AC, Sawant AC, Kassamali et al. Clinical Presentation, Long-Term Follow-Up, and Outcomes of 1001 Arrhythmogenic Right Ventricular Dysplasia/Cardiomyopathy Patients and Family Members. Circ Cardiovasc Genet 2015;8, 437–446. [PubMed: 25820315]
5. Cerrone M, Remme CA, Tadros R, Bezzina CR, Delmar M. Beyond the One Gene-One Disease Paradigm: Complex Genetics and Pleiotropy in Inheritable Cardiac Disorders. Circulation 2019;140, 595–610. [PubMed: 31403841]
6. Cerrone M MJ, Lin, Zhao Y-T, Zhang, Agullo-Pascual E, Alvarado FJ, Dolgalev, Karathanos TV, Malkani, et al. Plakophilin-2 is required for transcription of genes that control calcium cycling and cardiac rhythm. Nature Comm 2017 8, 106.

7. Kim JC, Pérez-Hernández M, Alvarado FJ, Maurya SR, Montnach J, Yin Y, Zhang M, Lin X, Vasquez C, Heguy A et al. Disruption of Ca(2+)i Homeostasis and Cx43 Hemichannel Function in the Right Ventricle Precedes Overt Arrhythmogenic Cardiomyopathy in PKP2-Deficient Mice. Circulation 2019;140, 1015–1030. [PubMed: 31315456]
8. Marcus FI, McKenna WJ, Sherrill D, Basso C, Bauce B, Bluemke DA, Calkins H, Corrado D, Cox MGPJ, Daubert JP et al. Diagnosis of arrhythmogenic right ventricular cardiomyopathy/dysplasia: proposed modification of the task force criteria. Circulation 2010;121, 1533–1541. [PubMed: 20172911]
9. Heffler J, Shah PP, Robison P, Phyo S, Veliz K, Uchida K, Bogush A, Rhoades J, Jain R, Prosser BL. A Balance Between Intermediate Filaments and Microtubules Maintains Nuclear Architecture in the Cardiomyocyte. Circ Res 2020;126, e10–e26.
10. Ljubojevic S, Radulovic S, Leitinger G, Sedej S, Sacherer M, Holzer M, Winkler C, Pritz E, Mittler T, Schmidt A, et al. Early remodeling of perinuclear Ca2+ stores and nucleoplasmic Ca2+ signaling during the development of hypertrophy and heart failure. Circulation 2014;130, 244–255. [PubMed: 24928680]
11. Earle AJ, Kirby TJ, Fedorchak GR, Isermann P, Patel J, Iruvanti S, Moore SA, Bonne G, Wallrath LL, Lammerding J. Mutant lamins cause nuclear envelope rupture and DNA damage in skeletal muscle cells. Nat Mater 2020;19, 464–473. [PubMed: 31844279]
12. Denais CM, Gilbert RM, Isermann P, McGregor AL, te Lindert M, Weigelin B, Davidson PM, Friedl P, Wolf K, Lammerding J. Nuclear envelope rupture and repair during cancer cell migration. Science 2016;352, 353–358. [PubMed: 27013428]
13. Mah LJ, El-Osta A, Karagiannis TC. gammaH2AX: a sensitive molecular marker of DNA damage and repair. Leukemia 2010;24, 679–686. [PubMed: 20130602]
14. Linscheid N, Santos A, Poulsen PC, Mills RW, Calloe K, Leurs U, Ye JZ, Stolte C, Thomsen MB, Bentzen BH et al. Quantitative proteome comparison of human hearts with those of model organisms. PLoS Biol 2021;19, e3001144. [PubMed: 33872299]
15. Linscheid N, Poulsen PC, Pedersen ID, Gregers E, Svendsen JH, Olesen MS, Olsen JV, Delmar M, Lundby A. Quantitative Proteomics of Human Heart Samples Collected In Vivo Reveal the Remodeled Protein Landscape of Dilated Left Atrium Without Atrial Fibrillation. Mol Cell Proteomics 2020;19, 1132–1144. [PubMed: 32291283]
16. Thompson A, Schäfer J, Kuhn K, Kienle S, Schwarz J, Schmidt G, Neumann T, Johnstone R, Mohammed AK, Hamon C. Tandem mass tags: a novel quantification strategy for comparative analysis of complex protein mixtures by MS/MS. Anal Chem 2003;75, 1895–1904. [PubMed: 12713048]
17. Paulo JA, Gygi SP. mTMT: An Alternative, Nonisobaric, Tandem Mass Tag Allowing for Precursor-Based Quantification. Anal Chem 2019;91, 12167–12172 [PubMed: 31490667]
18. Subramanian A, Tamayo P, Mootha VK, Mukherjee S, Ebert BL, Gillette MA, Paulovich A, Pomeroy SL, Golub TR, Lander ES et al. Gene set enrichment analysis: a knowledge-based approach for interpreting genome-wide expression profiles. Proc Natl Acad Sci U S A 2005;102, 15545–15550,. [PubMed: 16199517]
19. Liberzon A, Birger C, Thorvaldsdóttir H, Ghandi M, Mesirov JP, Tamayo P. The Molecular Signatures Database (MSigDB) hallmark gene set collection. Cell Syst 2015;1, 417–425. [PubMed: 26771021]
20. Reid DA, Reed PJ, Schlachetzki JCM, Nitulescu II, Chou G, Tsui EC, Jones JR, Chandran S, Lu AT, McClain CA et al. Incorporation of a nucleoside analog maps genome repair sites in postmitotic human neurons. Science 2021;372, 91–94. [PubMed: 33795458]
21. Kartenbeck J, Franke WW, Moser JG, Stoffels U. Specific attachment of desmin filaments to desmosomal plaques in cardiac myocytes. EMBO J 1983;2, 735–742. [PubMed: 6416832]
22. Cerrone M, Marron-Linares G, van Opbergen CJM, Costa S, Bourfiss M, Perez-Hernandez M, Schlamp F, Sanchis F, Malkani K, Drenkova K, et al. Role of Plakiophilin-2 expression on the exercise-related progression of arrhythmogenic right ventricular cardiomyopathy: A translational study. European Heart Journal 2021;43(12):1251–1264.
23. Srinivas US, Tan BWQ, Vellayappan BA, Jeyasekharan AD. ROS and the DNA damage response in cancer. Redox Biol 2019;25, 101084. [PubMed: 30612957]

24. Ahuja P, Wanagat J, Wang Z, Wang Y, Liem DA, Ping P, Antoshechkin IA, Margulies KB, Maclellan WR. Divergent mitochondrial biogenesis responses in human cardiomyopathy. Circulation 2013;127, 1957–1967. [PubMed: 23589024]
25. Perez-Hernandez M, Marrón-Liñares GM, Schlamp F, Heguy A, van Opbergen CJM, Mezzano V, Zhang M, Liang FX, Cerrone M, Delmar M. Transcriptomic Coupling of PKP2 With Inflammatory and Immune Pathways Endogenous to Adult Cardiac Myocytes. Front Physiol 2020;11, 623190. [PubMed: 33536940]
26. Sundaresan NR, Gupta M, Kim G, Rajamohan SB, Isbatan A, Gupta MP.Sirt3 blocks the cardiac hypertrophic response by augmenting Foxo3a-dependent antioxidant defense mechanisms in mice. J Clin Invest 2009;119, 2758–2771. [PubMed: 19652361]
27. Cheung KG, Cole LK, Xiang B, Chen K, Ma X, Myal Y, Hatch GM, Tong Q, Dolinsky VW. Sirtuin-3 (SIRT3) Protein Attenuates Doxorubicin-induced Oxidative Stress and Improves Mitochondrial Respiration in H9c2 Cardiomyocytes. J Biol Chem 2015;290, 10981–10993. [PubMed: 25759382]
28. Kerr M, Miller JJ, Thapa D, Stiewe S, Timm KN, Aparicio CNM, Scott I, Tyler DJ, Heather LC. Rescue of myocardial energetic dysfunction in diabetes through the correction of mitochondrial hyperacetylation by honokiol. JCI Insight 2020;5.
29. Pillai VB, Samant S, Sundaresan NR, Raghuraman H, Kim G, Bonner MY, Arbiser JL, Walker DI, Jones DP, Gius D et al. Honokiol blocks and reverses cardiac hypertrophy in mice by activating mitochondrial Sirt3. Nat Commun 2015;6, 6656. [PubMed: 25871545]
30. Akdis D, Medeiros-Domingo A, Gaertner-Rommel A, Kast JI, Enseleit F, Bode P, Klingel K, Kandolf R, Renois F, Andreoletti L et al. Myocardial expression profiles of candidate molecules in patients with arrhythmogenic right ventricular cardiomyopathy/dysplasia compared to those with dilated cardiomyopathy and healthy controls. Heart Rhythm 2016;13, 731–741. [PubMed: 26569459]
31. Kim C, Wong J, Wen J, Wang S, Wang C, Spiering S, Kan NG, Forcales S, Puri PL, Leone TC et al. Studying arrhythmogenic right ventricular dysplasia with patient-specific iPSCs. Nature 2013;494, 105–110. [PubMed: 23354045]
32. Valente M, Calabrese F, Thiene G, Angelini A, Basso C, Nava A, Rossi L. In vivo evidence of apoptosis in arrhythmogenic right ventricular cardiomyopathy. Am J Pathol. 1998;152(2):479–84. [PubMed: 9466574]
33. Nishikawa T, Ishiyama S, Nagata M, Sakomura Y, Nakazawa M, Momma K, Hiroe M, Kasajima T. Programmed cell death in the myocardium of arrhythmogenic right ventricular cardiomyopathy in children and adults. Cardiovasc Pathol. 1999;8(4):185–9. [PubMed: 10724522]
34. Capetanaki Y, Bloch RJ, Kouloumenta A, Mavroidis M, Psarras S. Muscle intermediate filaments and their links to membranes and membranous organelles. Exp Cell Res 2007;313, 2063–2076. [PubMed: 17509566]
35. Chelko SP, Keceli G, Carpi A, Doti N, Agrimi J, Asimaki A, Beti CB, Miyamoto M, Amat-Codina N, Bedja D et al. Exercise triggers CAPN1-mediated AIF truncation, inducing myocyte cell death in arrhythmogenic cardiomyopathy. Sci Transl Med 2021;13(581):eabf0891. [PubMed: 33597260]
36. Nicolas-Avila JA, Lechuga-Vieco AV, Esteban-Martínez L, Sánchez-Díaz M, Díaz-García E, Santiago DJ, Rubio-Ponce A, Li JL, Balachander A, Quintana JA et al. A Network of Macrophages Supports Mitochondrial Homeostasis in the Heart. Cell 2020;183, 94–109 e123. [PubMed: 32937105]
37. Chelko SP, Asimaki A, Lowenthal J, Bueno-Beti C, Bedja D, Scalco A, Amat-Alarcon N, Andersen P, Judge DP, Tung L et al. Therapeutic Modulation of the Immune Response in Arrhythmogenic Cardiomyopathy. Circulation 2019;140, 1491–1505. [PubMed: 31533459]
38. Rouhi L, Cheedipudi SM, Chen SN, Fan S, Lombardi R, Chen X, Coarfa C, Robertson MJ, Gurha P, Marian AJ. Haplo-insufficiency of Tmem43 in cardiac myocytes activates the DNA damage response pathway leading to a Late-Onset Senescence-Associated pro-fibrotic cardiomyopathy. Cardiovasc Res, 2020; 117(11):2377–2394.
39. Chen SN, Lombardi R, Karmouch J, Tsai JY, Czernuszewicz G, Taylor MRG, Mestroni L, Coarfa C, Gurha P, Marian AJ. DNA Damage Response/TP53 Pathway Is Activated and Contributes to the Pathogenesis of Dilated Cardiomyopathy Associated With LMNA (Lamin A/C) Mutations. Circ Res 2019;124, 856–873. [PubMed: 30696354]

40. Quarta G, Syrris P, Ashworth M, Jenkins S, Zuborne Alapi K, Morgan J, Muir A, Pantazis A, McKenna WJ, Elliott PM. Mutations in the Lamin A/C gene mimic arrhythmogenic right ventricular cardiomyopathy. Eur Heart J 2012;33, 1128–1136. [PubMed: 22199124]
41. Haywood AF, Merner ND, Hodgkinson KA, Houston J, Syrris P, Booth V, Connors S, Pantazis A, Quarta G, Elliott P et al. Recurrent missense mutations in TMEM43 (ARVD5) due to founder effects cause arrhythmogenic cardiomyopathies in the UK and Canada. Eur Heart J 2013;34, 1002–1011. [PubMed: 23161701]
42. Numaga-Tomita T, Oda S, Nishiyama K, Tanaka T, Nishimura A, Nishida M. TRPC channels in exercise-mimetic therapy. Pflugers Arch 2019;471, 507–517. [PubMed: 30298191]
43. Li N, Guenancia C, Rigal E, Hachet O, Chollet P, Desmoulins L, Leloup C, Rochette L, Vergely C. Short-term moderate diet restriction in adulthood can reverse oxidative, cardiovascular and metabolic alterations induced by postnatal overfeeding in mice. Sci Rep 2016;6, 30817. [PubMed: 27465434]
44. Towbin JA, McKenna WJ, Abrams DJ, Ackerman MJ, Calkins H, Darrieux FCC, Daubert JP, de Chillou C, DePasquale EC, Desai MY et al. 2019 HRS expert consensus statement on evaluation, risk stratification, and management of arrhythmogenic cardiomyopathy: Executive summary. Heart Rhythm 2019;16, e373–e407. [PubMed: 31676023]
45. Zecha J, Satpathy S, Kanashova T, Avanessian SC, Kane MH, Clauser KR, Mertins P, Carr SA, Kuster B. TMT Labeling for the Masses: A Robust and Cost-efficient, In-solution Labeling Approach. Mol Cell Proteomics 2019;18, 1468–1478. [PubMed: 30967486]
46. Robinson MD, McCarthy DJ, Smyth GK. edgeR: a Bioconductor package for differential expression analysis of digital gene expression data. Bioinformatics 2010;26, 139–140. [PubMed: 19910308]
47. Subramanian A, Tamayo P, Mootha VK, Mukherjee S, Ebert BL, Gillette MA, Paulovich A, Pomeroy SL, Golub TR, Lander ES et al. Gene set enrichment analysis: a knowledge-based approach for interpreting genome-wide expression profiles. Proc Natl Acad Sci U S A 2005;102, 15545–15550. [PubMed: 16199517]
48. Liberzon A, Birger C, Thorvaldsdóttir H, Ghandi M, Mesirov JP, Tamayo P. The Molecular Signatures Database (MSigDB) hallmark gene set collection. Cell Syst 2015;1, 417–425. [PubMed: 26771021]
49. Pan J, Lee Y, Zhang Q, Xiong D, Wan TC, Wang Y, You M. Honokiol Decreases Lung Cancer Metastasis through Inhibition of the STAT3 Signaling Pathway. Cancer Prev Res (Phila). 2017;10(2):133–141. [PubMed: 27849557]
50. Pérez-Hernández M, Leo-Macias A, Keegan S, Jouni M, Kim JC, Agullo-Pascual E, Vermij S, Zhang M, Liang FX, Burridge P et al. Structural and Functional Characterization of a Na(v)1.5-Mitochondrial Couplon. Circ Res 2021;128, 419–432. [PubMed: 33342222]
51. Sato PY, Chuprun JK, Grisanti LA, Woodall MC, Brown BR, Roy R, Traynham CJ, Ibetti J, Lucchese AM, Yuan A, et al. Restricting mitochondrial GRK2 post-ischemia confers cardioprotection by reducing myocyte death and maintaining glucose oxidation. Sci Signal. 2018;11(560):eaau0144. [PubMed: 30538174]
52. Chollet F Xception: Deep Learning with Depthwise Separable Convolutions. arXiv:1610.02357.

Clinical perspective

What is new?

- A multidisciplinary study including ARVC human samples as well as PKP2-deficient murine and hiPSC-CMs with proteomics and functional analysis at unprecedented depth.
- We associate loss or mutations in PKP2 with a disruption of nuclear envelope integrity that precedes or parallels metabolic dysfunction and alters the transcriptional and proteome profile.

What are the clinical implications?

- Advanced knowledge on the molecular substrates linking PKP2 to ARVC.
- We identify novel potential actionable targets to ameliorate the progression of the disease.

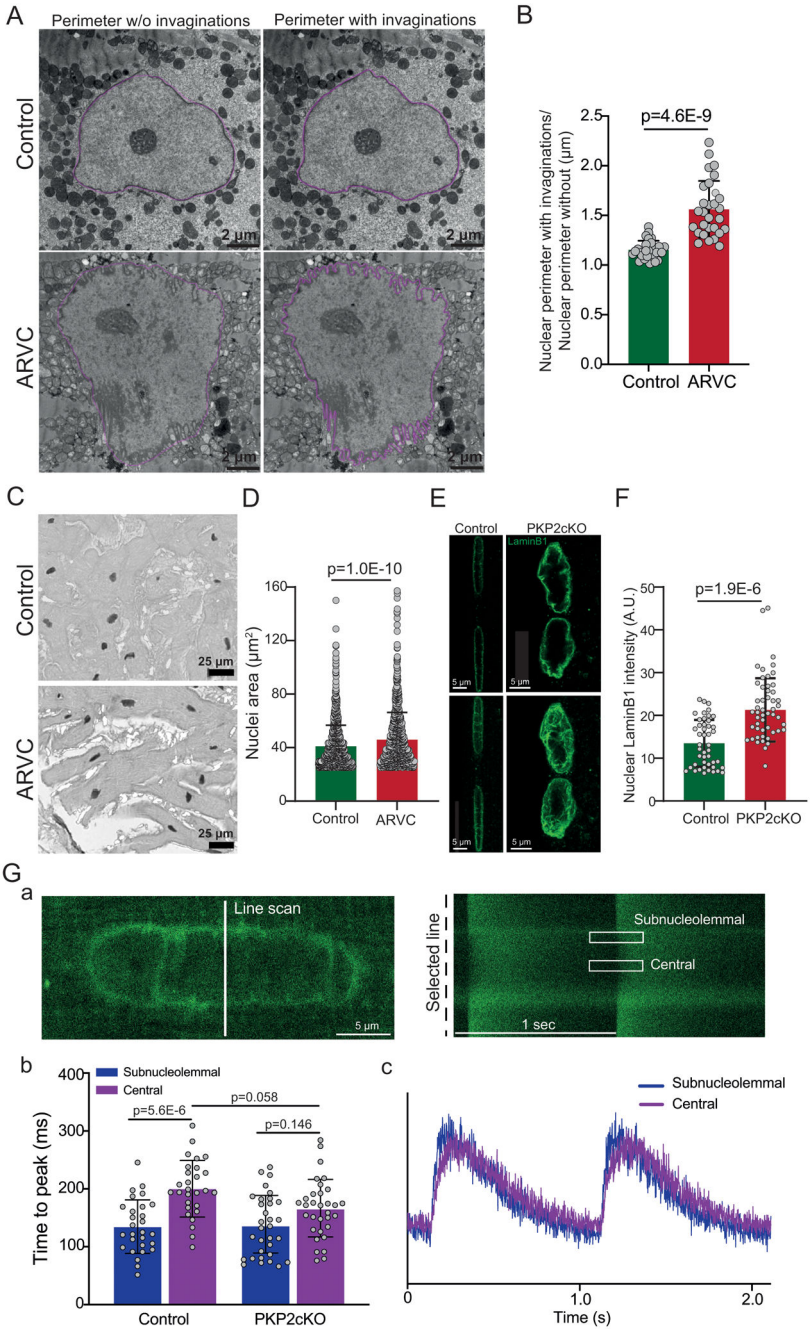

Figure 1: Structural and functional modifications of the nuclear envelope in ARVC patients and in PKP2-deficient heart cells.

A: TEM images of the nuclei of cardiac myocytes obtained from a control (top) and an ARVC patient (bottom) biopsy sample. Purple line marks the contour of the nuclear envelope. The ratio of the perimeter measured while accounting for invaginations over the perimeter measured without invaginations is shown in **B**. Each dot corresponds to 1 nucleus. Control n=28 nuclei from three control patients; ARVC n=28 nuclei from five ARVC patients. Columns/bars represent mean and standard deviation, respectively. Statistical test: Linear Mixed Effects Model. **C**: Histological sections obtained from a control (top) and

an ARVC patient (bottom) biopsy Haematoxylin-stained to mark the nuclei. Images were digitally pre-processed by an experienced cardiac pathologist to remove nuclei from non-myocyte cells (see Supplementary Figure S4). **D**: Quantitative analysis of sections obtained from 3 controls and 5 ARVC patient samples showing larger nuclei area in the ARVC group. Columns/bars represent mean and standard deviation. Each dot corresponds to 1 nucleus. Statistical test: Generalized Linear Mixed Effects Model. **E**: Confocal stacked immunofluorescence images of laminB1, marking the nuclear envelope of control (top) and of PKP2-deficient myocytes obtained from PKP2cKO mice. Top images show a single plane, while bottom images display the whole stack. Notice the increased invaginations in the PKP2cKO nuclei. Quantitative analysis of total nuclear laminB1 intensity is shown in **F**. Intensity is measured between 0 and 255. Each symbol represents one nucleus. Control, n=42 nuclei from N=4 mice; PKP2cKO , n=42 nuclei from N=4 mice. Columns and bars represent mean and standard deviation values, respectively. Statitical test: Generalized Linear Mixed Effects Model. **G**: Line confocal Ca^{2+} imaging of the nuclear and perinuclear region of murine cardiomyocytes from control and PKP2cKO myocytes. **Ga**: Image of the nucleus of a control myocyte stained with the Ca^{2+} indicator Fluo-8. The position of the line scan is indicated by the white line in the middle and a time-space plot of the fluorescence is presented in the right. The average time to upstroke measured from the subnucleolemmal and from the central region of the nucleus are shown in **Gb** and examples of the transients are shown in **Gc**. In **Gb** and **Gc**, blue represents data/traces from the subnucleolemmal and purple from the central regions. Number of nuclei measured are indicated in the columns. Data collected from Controls, n=28 cells, N=3 mice; PKP2cKO, n=32 cells, N=3 mice. Columns indicate mean and bars, standard deviation of the mean. P values indicated by the horizontal bars. Statistical test: Linear Mixed Effects Model.

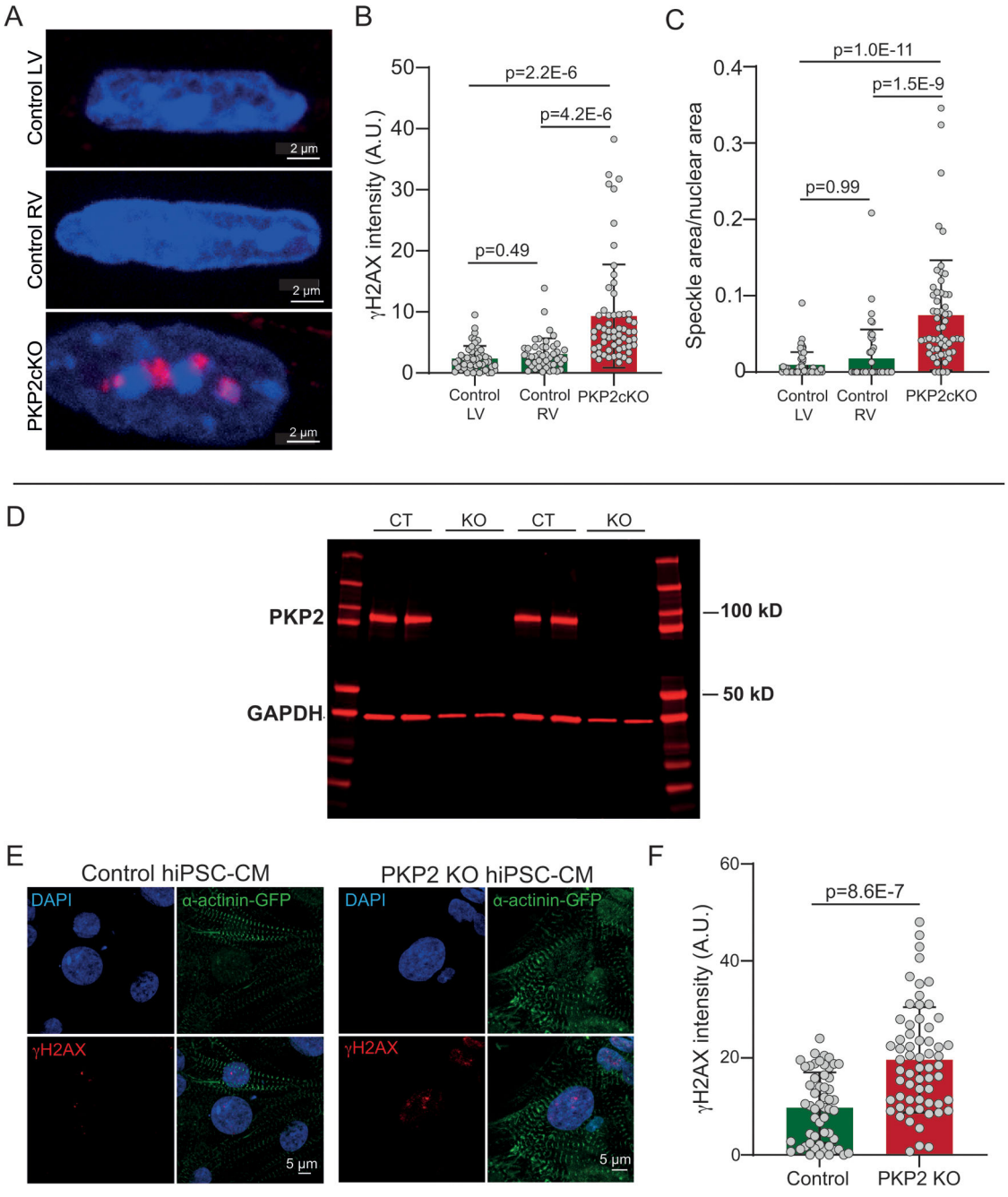

Figure 2: γH2AX in cardiac myocytes deficient in PKP2.

A: Representative images of adult murine cardiac myocyte nuclei from control left and right ventricular myocytes (top and middle) and from a PKP2cKO myocyte, immunostained for γH2AX (red) and with DAPI (blue) as a nuclear marker. Quantitative analysis of γH2AX intensity is shown in **B** and quantification of the area occupied by the speckles formed by γH2AX is shown in **C**. In B and C each symbol represents data from one nucleus. Control LV n=52 nuclei, N=4 mice; Control RV n=46 nuclei, N= 4 mice; and PKP2cKO n=60 nuclei, N= 6 mice. P values as per Generalized Linear Mixed Effects Model are indicated in the plot. Panels D-F show data from human induced pluripotent

stem cell-derived cardiomyocytes (hiPSC-CMs). **D**: Western blot for PKP2 obtained from cells either Control hiPSC-CMs or after PKP2 KO. **E**: Representative images obtained from Control and PKP2 KO hiPSC-CMs expressing α-actinin -GFP (green) and stained for DAPI (blue) and γH2AX (red). **F:** Quantitative analysis of γH2AX intensity obtained from 55 control and 62 PKP2KO cells from 3 separate batches. Each symbol represents one nucleus. Horizontal bar indicates statistical significance, as determined by a Mann-Whitney test.

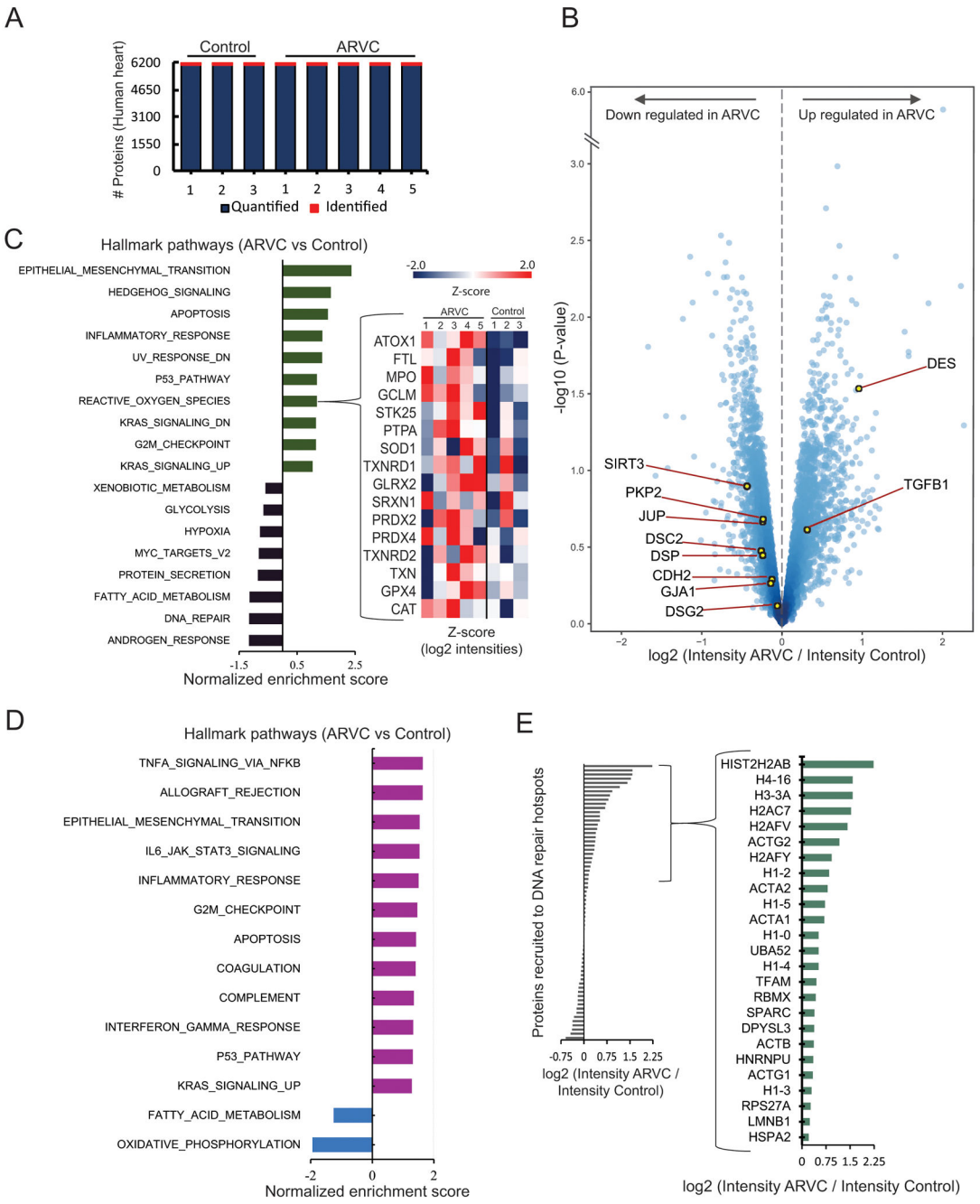

Figure 3: Differential proteomics and transcriptomics analyses of data from human heart biopsies from ARVC patients and healthy relatives (control).

A: Number of proteins identified (red) and quantified (blue) from proteomics measurements from five ARVC and three control heart samples. **B**: Volcano plot representation of protein abundances in ARVC patient hearts compared to controls. All points represent a protein. The negative logarithm (base 10) of LIMMA based empirical Bayes moderated test statistics derived p-value is shown as a function of logarithmic (base 2) ratios of protein intensities in ARVC patients relative to controls. Yellow points highlight proteins of the intercalated disc and the mitochondrial NAD^+-dependent deacetylase Sirt3 (downregulated in ARVC) as

well as desmin (Des) and Tgfb1 (upregulated in ARVC). **C**: Hallmark pathway analysis underrepresented (negative numbers) or over-represented (positive numbers) in ARVC hearts. Proteins in the “reactive oxygen species” pathway are highlighted, and individual data points illustrated by the heatmap on the right. **D**: Hallmark pathway analysis from transcriptomics data obtained from the same patients. Same conventions as in C; notice consistency with proteomics data in upregulation of apoptosis and DNA damage response pathways, and downregulation of oxidative phosphorylation. **E**: Analysis of the differential proteomics dataset for proteins reported as part of DNA repair hotspots.[20] Abundance differences for all proteins part of the repair hotspots in ARVC hearts compared to controls are shown. Details are highlighted for proteins with increased abundances in hearts of ARVC patients.

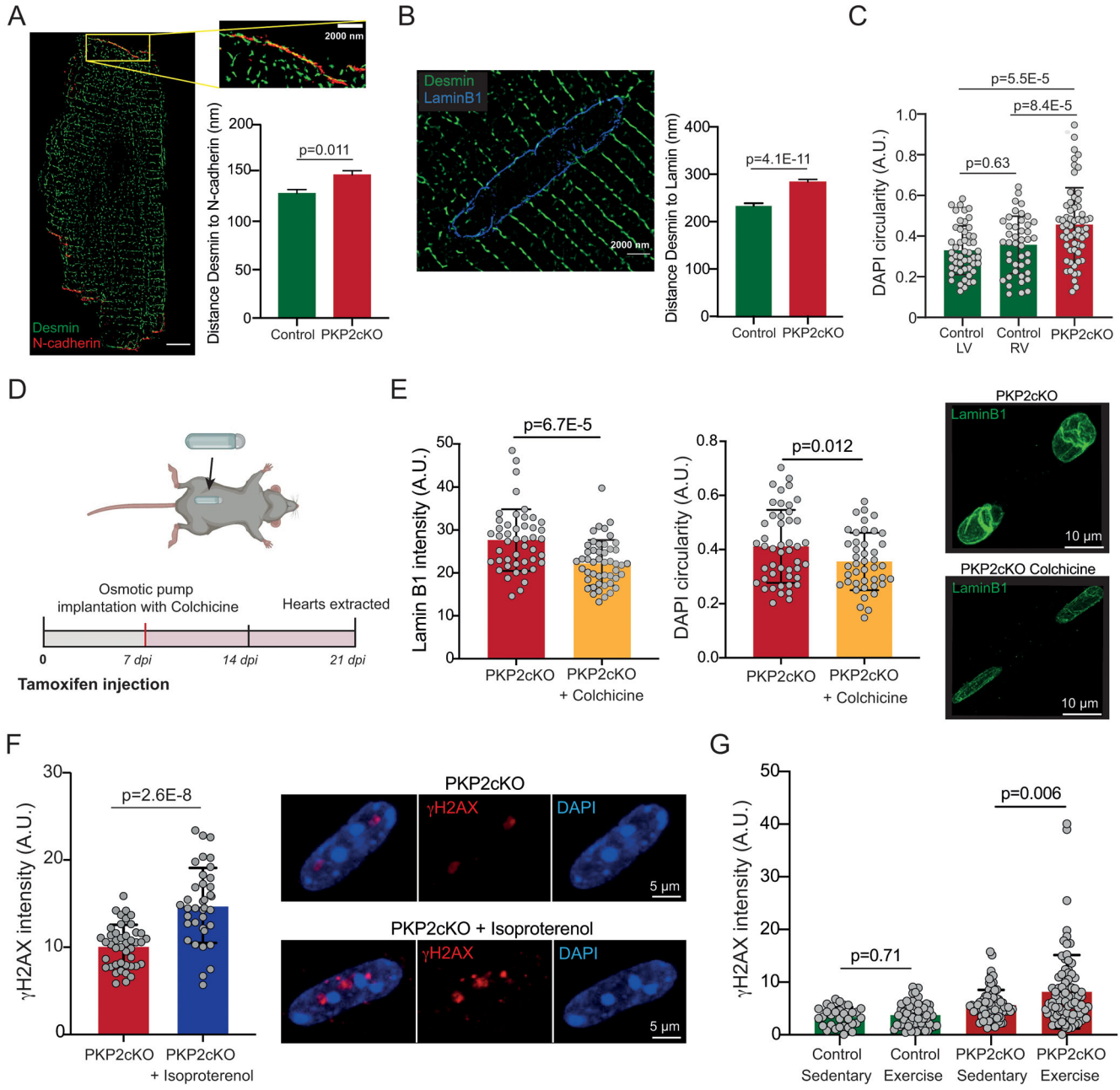

Figure 4: Desmin abundance/localization, nuclear morphology and DNA damage response under conditions of mechanical stress in PKP2 deficient adult ventricular myocytes.

A: Stochastic optical reconstruction microscopy (STORM) image of an adult ventricular myocyte stained for Desmin (green) and N-cadherin as marker of cell end (red). Yellow-boxed area is enlarged to the right. Distances from Desmin to nearest N-cadherin cluster were measured. Columns indicate mean and bars, standard deviation of the mean. The complete data distribution is presented in Supplemental Figure 8A. The mean distance is significantly greater in PKP2cKO cells. Statistical test: Generalized Linear Mixed Effects Model. Control: n= 2265 clusters from 22 images, N=4 mice. PKP2cKO: n=2398 clusters from 26 images, N =5 mice. **B**: STORM image of an adult ventricular myocyte stained for

Desmin (green) and LaminB1 as marker of the nuclear envelope (blue). We measured the distances from Desmin to the nearest LaminB1 cluster. Columns indicate mean and bars, standard deviation of the mean. The mean distance is significantly greater in PKP2cKO cells. Statistical test: Generalized Linear Mixed Effects Model. Control: n=3901 clusters from 15 images, N=3 mice. PKP2cKO: n=4202 clusters from 16 images, N=4 mice. **C**: Measurements of nuclear circularity from DAPI stained control and PKP2cKO myocytes. Nuclear circularity was measured as the ratio nuclear width/nuclear length of Control LV (n= 52 nuclei, N=4 mice), Control RV (n= 43 nuclei, N=4 mice) and PKP2cKO (n=60 nuclei, N=6 mice) myocytes. Statistical test: Generalized Linear Mixed Effects Model. **D**: Timeline of colchicine experiment: osmotic pumps containing either colchicine (0.4 mg/kg/d) or control vehicle (saline) were intraperitoneally inserted through a small abdominal incision, in PKP2cKO mice at 7 days post-TAM (7 dpi). Pumps were maintained for 14 days. **E**: Quantitative analysis of total nuclear laminB1 intensity from colchicine or vehicle-treated mice. Intensity is measured between 0 and 255. Each symbol represents one nucleus. PKP2cKO, n=46 nuclei from N=4 mice; PKP2cKO+colchicine, n=48 nuclei from N=4 mice. Columns and bars represent mean and standard deviation values, respectively. Statistical test: Linear Mixed Effects Model. Representative images of LaminB1 are shown on the right. **F**: DAPI (blue) and γH2AX staining (red) of nuclei from cardiomyocytes isolated from PKP2cKO hearts subjected to boluses of Isoproterenol or vehicle. Quantitative analysis of γH2AX intensity is presented in the left. Numbers of nuclei/mice analyzed were 44/3 for PKP2cKO and 37/3 for PKP2cKO+Isoproterenol. Statistical Test: Linear Mixed Effects Model. **G**: Quantitative analysis of γH2AX intensity from nuclei obtained from mice sedentary or subjected to a six-week treadmill running program. γH2AX intensity from ventricular myocytes of sedentary control (n=31 nuclei, N=3 mice), exercised control (n=57 nuclei, N=4 mice), sedentary PKP2cKO (n=76 nuclei, N=4 mice) and exercised PKP2cKO mice (n=82 nuclei, N=5 mice) are shown. Statistical significance is reported in the figure as evaluated by Linear Mixed Effects Model (Control Sedentary vs Control Exercise) or Generalized Linear Mixed Effects Model (PKP2cKO Sedentary vs PKP2cKO Exercise).

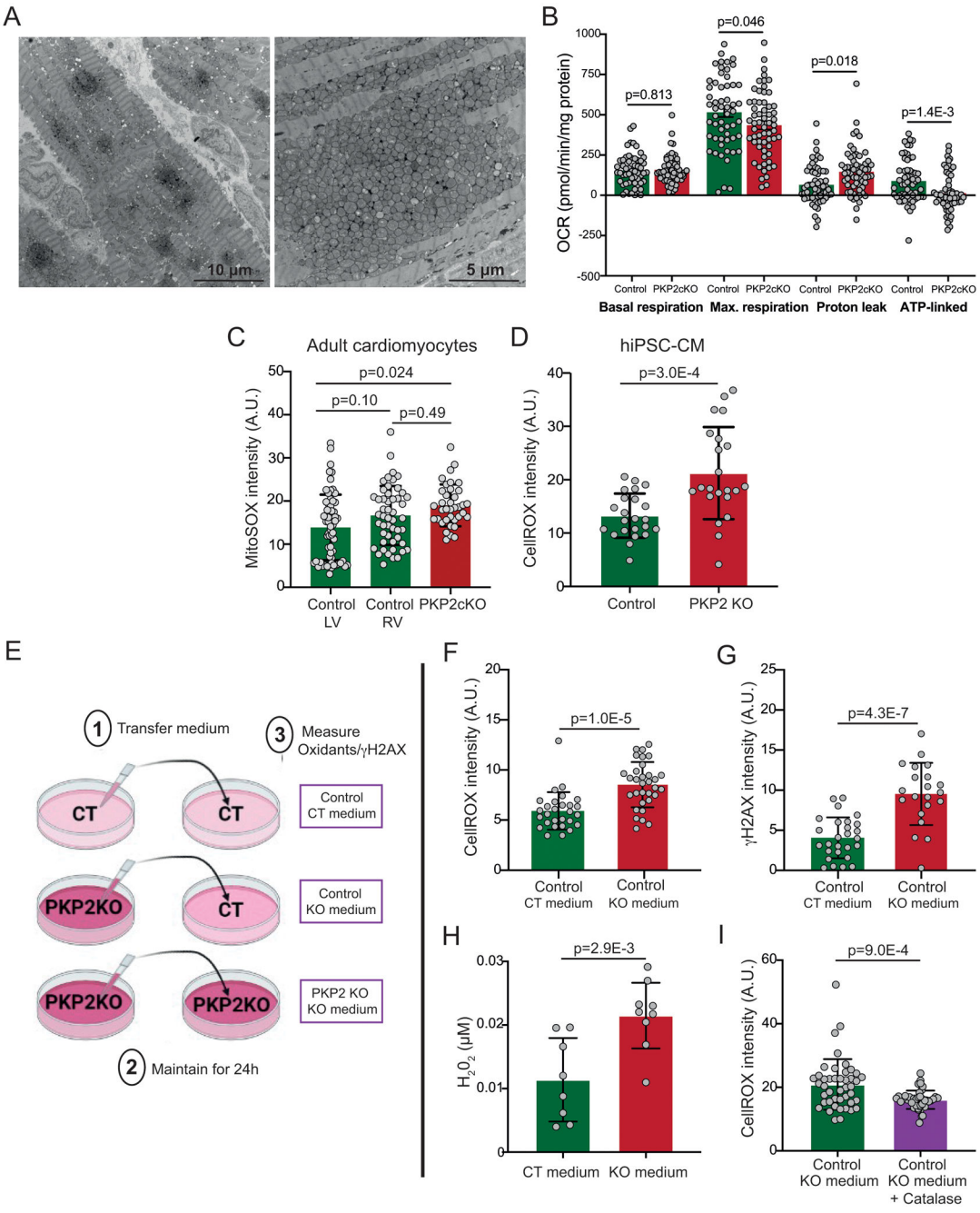

Figure 5: Mitochondrial morphology, function and oxidant production in PKP2-deficient hearts/ myocytes.

A: TEM images obtained from a right ventricular septal biopsy tissue collected from an ARVC patient. Notice the large accumulation of mitochondria within the cells. **B**: Seahorse oxygen consumption rates (OCRs) were measured in isolated adult cardiomyocytes from control and PKP2cKO mice. Numbers of mice/recordings analyzed were, for control, N=3 mice; n=56 recordings and for PKP2cKO, N=3 mice; n=61 recordings. Columns and bars represent mean and standard deviation values, respectively. Statistical test for basal respiration, proton leak and ATP-linked: Generalized Linear Mixed Effects Model.

Statistical test for maximal respiration: Linear Mixed Effects Model. **C**: Quantitative analysis of superoxide radical anion radical ($O_2^{\bullet -}$) formation in MitoSOX-loaded ventricular myocytes dissociated from control right and left ventricular tissue (control LV; control RV) and from a PKP2cKO heart. Numbers of cells/mice analyzed were for control (N=5 mice; n=64 LV; n=50 RV) and PKP2cKO (N=3 mice; n=37 cells). Statistical test: Linear Mixed Effects Model. **D:** Quantitative analysis of oxidant levels measured in cellROX-loaded hiPSC-CMs (n=23 images, 3 separate batches) and PKP2 KO hiPSC-CMs (n=22 images, 3 separate batches) (measured only in the GFP+ cells). Statistical test: Student's t-test. Each symbol represents one cell; columns indicate average values and bars, standard deviation. **E**: Diagram explaining the transfer media experiment in hiPSC-CMs. Figure created with BioRender.com. **F**: Average cellROX intensity recorded from control hiPSC-CMs that received conditioned media from other control cells (left column; CT-CT), or from PKP2KO cells (middle column; CT-KO). Each symbol represents one image; n= 27 and 32 images analyzed for CT-CT and CT-KO respectively from 4 separate bacthes. Statistical test: Student's t-test. **G**: Same experimental protocol as in **F**, but cells were fixed and stained for γH2AX. Each symbol represents one cell; n=27 and 21 cells, analyzed for CT-CT and CT-KO respectively, from 3 separate batches. Statistical test: Student's t-test. **H:** Measurement of H_2O_2 concentration in the conditioned media supernatant collected from culture dishes containing hiPSC-CMs control (left column, n=8 culture dishes run in triplicates) or PKP2KO hiPSC-CMs (right column, n=9 culture dishes run in triplicates). Statistical test: Student's t-test **I:** Quantitative analysis of oxidant levels in cellROX-loaded hiPSC-CMs incubated with the soluble fraction of the medium from PKP2KO hiPSC-CMs culture dish treated either with catalase (10 μmol/L; right column) or with vehicle (left column). Each symbol represents one cell; n=44 from 4 separate batches analyzed for each condition. Statistical test: Mann-Whitney Test. For all graphs, columns indicate average values and bars, standard deviation.

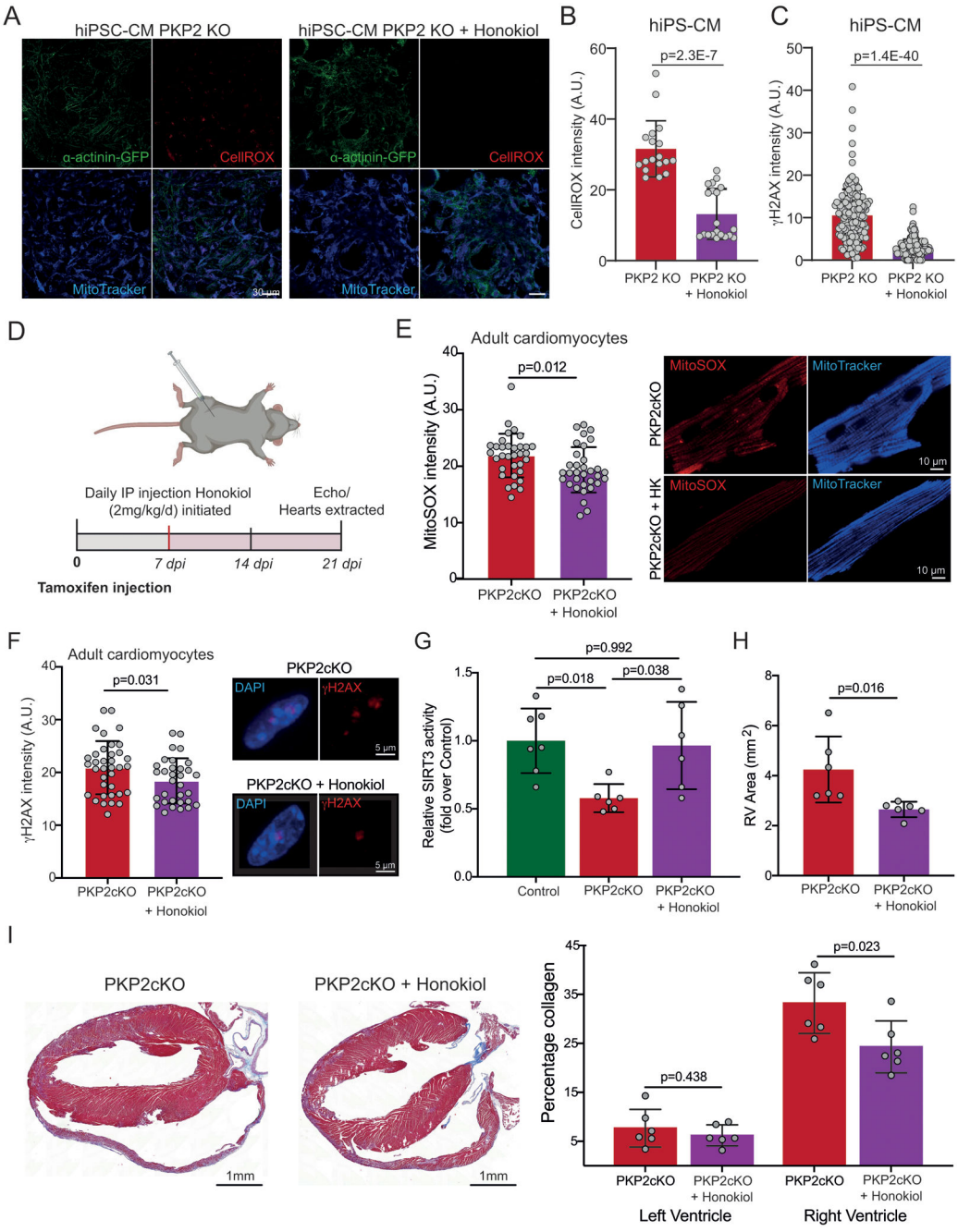

Figure 6: Honokiol exposure to PKP2KO hiPSC-CMs and Honokiol treatment of PKP2cKO mice reduces oxidant levels, DNA damage phenotypes and prevents right ventricular remodeling.

A. Representative confocal images of PKP2 KO hiPSC-CMs stained with cellROX (red) and MitoTracker (blue) expressing α-actinin-GFP (green), with and without 10 μmol/L Honokiol treatment for 24 hours. MitoTracker was used to identify mitochondria and cellROX as an indicator of oxidant production. Quantitative analysis of cellROX intensity is shown in **B**. hiPSC-CM PKP2 KO, n=18 images. + Honokiol, n=20 images; from 3 separate batches. Statistical test: Mann-Whitney test. **C**. Quantitative analysis of γH2AX intensity of hiPSC-CM PKP2 KO, n=170 nuclei. + Honokiol, n=193 nuclei; from 3 separate

batches. Statistical test: Mann-Whitney test. **D:** Experimental timeline for chronic treatment of PKP2cKO mice with Honokiol: Honokiol (2mg/kg/day) or control vehice (saline) was intraperitoneally injected into PKP2cKO mice for 14 consecutive days. Treatment started at 7 days post-TAM (dpi) and at 21 dpi, mice were subjected to echocardiography and hearts extracted for histology and cellular experiments. **E:** Representative confocal images of PKP2cKO ventricular myocytes stained with MitoSOX (red) and MitoTracker (blue) are shown. Quantitative analysis of MitoSOX intensity is shown in the bargraph on the left. Numbers of cells/mice were 33/3 for control and 33/3 for PKP2cKO. Statistical test: Linear Mixed Effects Model.. **F.** Same experimental protocol as in **E**, but cells were fixed and immunostained for γH2AX (red) and DAPI (blue). PKP2cKO n=36 cells, N=3 mice; +Honokiol n=32 cells, N=3 mice. Quantification of the γH2AX intensity is shown in the bargraph on the left. Statistical test: Linear Mixed Effects Model. **G**. SIRT3 activity was measured *in vitro* in isolated cardiac mitochondria from control, PKP2cKO and Honokiol treated PKP2cKO mice (N=7, 6 and 6 mice, respectively). Statistical test: one way ANOVA Tukey's multiple comparisons test. **H**. Right ventricular (RV) free wall area measurements by B-mode long axis echocardiography, in PKP2cKO mice with and without chronic Honokiol treatment (N=6 mice for PKP2cKO and 6 for PKP2cKO+Honokiol). Statistical test: Student's t test. **I**. Representative images of Masson Trichrome stained four-chamber view sections of PKP2cKO and PKP2cKO+Honokiol hearts. Quantitative analysis of percentage collagen is shown on the right. N=6 mice for PKP2cKO and N=6 for PKP2cKO+Honokiol. Statistical test: Student's t-test. For all graphs, columns indicate average values and bars, standard deviation.

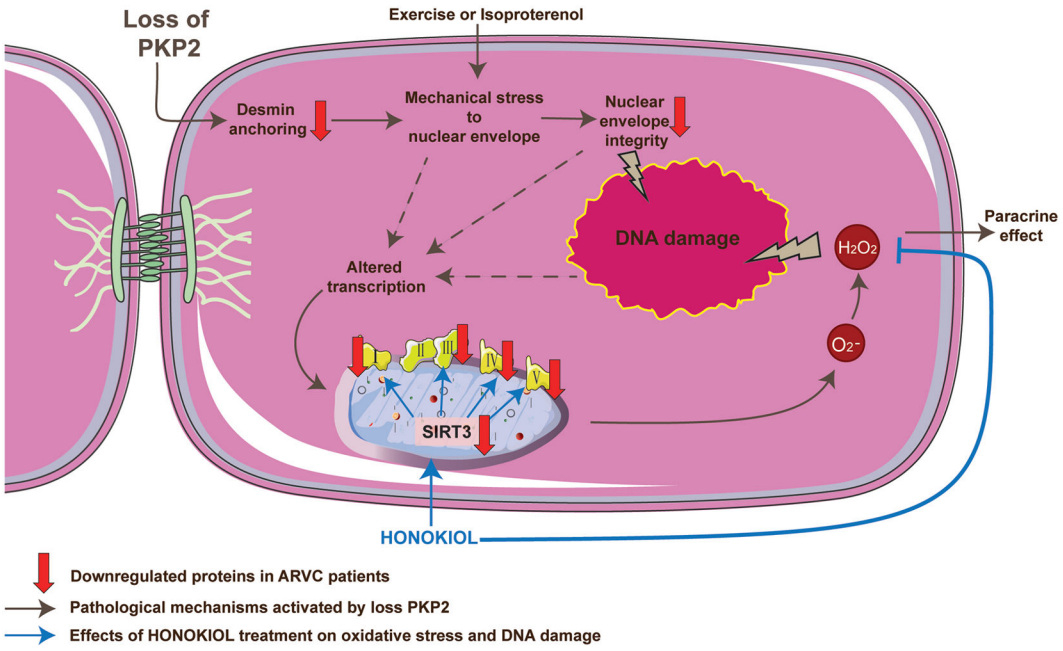

Figure 7: Working model of cardiomyocyte remodeling in PKP2-dependent arrhythmogenic right ventricular cardiomyopathy (ARVC).

Our data show that a PKP2 deficit in an adult heart disrupts nuclear envelope morphology and its barrier function, leading to DNA damage and altered transcription. We further show that this phenomenon is facilitated by exercise or increased adrenergic tone, and it is associated with a separation of the intermediate filament desmin from its anchoring points both at the cell end and at the nuclear envelope. We also demonstrate that, in parallel, transcriptional reprogramming includes reduced expression of electron transport chain proteins and consequent enhanced formation of superoxide radical anions, $O_2^{\bullet -}$ yielding increased H_2O_2. We report that the H_2O_2 extruded from PKP2 deficient myocytes can cause DNA damage in distal PKP2-expressing cells and show that treatment with Honokiol, a natural product that among its effects is to activate the mitochondrial deacetylase Sirt3, reduces oxidant formation and DNA damage in myocytes deficient in PKP2, suggesting that reduction of oxidant levels can be considered a therapeutic goal for patients with ARVC.

Table 1.

Right and left ventricular dimensions, volumes, and indicators of systolic functioning in subjects with arrhythmogenic right ventricular cardiomyopathy

ID	Sex	Height (cm)	Weight (kg)	LVEDd (mm)	LV EDV (ml)	LV ESV (ml)	LVEF (%)	GLS (%)	RV base (mm)	RV length (mm)	RV mid (mm)	TAPSE (mm)	Arrhythmias
A	M	193	93	58	172	92	46	−16.0	57	90	56	17	VF, VT
B	M	185	90	54	162	63	61	−22.8	38	75	39	25	VT, AF
C	M	188	69	46	154	60	61	−19.0	53	86	39	26	VT
D	M	191	102	57	214	87	59	−20.0	46	73	42	29	none
E	M	178	103	58	152	78	49	−15.7	50	77	42	16	VF, VT

Abbreviations: *AF* = atrial fibrillation, *EDd* = end-diastolic diameter, *EDV* = End-diastolic volume, *EF* = Ejection fraction, *ESV* = end-systolic volume, *GLS* = global longitudinal strain, LV = left ventricular, *RV* = right ventricular, *TAPSE* = Tricuspid annular plane excursion, *VF* = ventricular fibrillation, *VT* = sustained ventricular tachycardia.

Description: All echocardiography measures were from examinations performed on the day of the biopsy-procedure. Left ventricular volumetric measures are from 3D echocardiography. Measures of right ventricular dimensions are consistent with right ventricular dilation in subjects A, C, D and E, while significant reduction of right ventricular systolic function was only present in subjects A and E. Left ventricular function was also mildly/borderline reduced in subjects A and E, but not enough to fulfil criteria for left ventricular systolic dysfunction and no heart failure symptoms were present.